2017

Growth and Characterization of Anisotropic Gase Semiconductor for Radiation Detection and Thz Applications

Haseeb Nazir
University of South Carolina

Follow this and additional works at: http://scholarcommons.sc.edu/etd

Part of the Electrical and Computer Engineering Commons

Recommended Citation

GROWTH AND CHARACTERIZATION OF ANISOTROPIC GASE SEMICONDUCTOR
FOR RADIATION DETECTION AND THZ APPLICATIONS

By

Haseeb Nazir

Bachelor of Science
University of South Carolina, 2011

Submitted in Partial Fulfillment of the Requirements

For the Degree of Master of Science in

Electrical Engineering

College of Engineering and Computing

University of South Carolina

2017

Accepted by:

Krishna C. Mandal, Director of Thesis

Bin Zhang, Reader

Cheryl L. Addy, Vice Provost and Dean of the Graduate School

DEDICATION

I dedicate this dissertation work to my beloved wife, Shafia Naeem and my respective parents. Their endless efforts and encouragement has nurtured my eagerness towards this goal. A special thanks to my wife, whose support and encouragement elevated me throughout.

ACKNOWLEDGEMENTS

First, I would pay my high gratitude to my advisor, Dr. Krishna C. Mandal, for giving me an opportunity to work in his group and has made this project possible. His mentorship, guidance, and endless support have truly inspired me to finish my graduate research.

Secondly, I would like to thank my committee members, Dr. Krishna C. Mandal and Dr. Bin Zhang for taking time out of their very busy schedule to oversee my work.

Finally I would like to thank my lab colleagues, Mr. Cihan Oner and Mr. Towhid A. Chowdhury for providing me help, support, and knowledge in the field and their invaluable experimental support in the laboratory. I am also indebted to Mr. Tim Hayes, MS, Dr. Ramesh Krishna, Dr. Sandip Das, and Dr. Pak O. Rahmi for their valuable work on crystal growth and characterization which made my research work easier than I thought. Without their support, it would not have been possible to complete this thesis work.

ABSTRACT

Anisotropic wide-bandgap gallium selenide (GaSe) crystals were grown using high purity (7N) Ga and zone refined (ZR) Se precursor materials. The crystal growth was performed using a modified vertical Bridgman method (VBM) with a slow crystallization from the melt and with a pre-determined temperature profile. The structure, surface morphology, and the composition of the grown crystals were characterized using x-ray diffraction (XRD), scanning electron microscopy (SEM), and energy dispersive analysis by x-rays (EDAX), respectively. Optical absorption and transmission properties were characterized and optical bandgap was determined. Electrical resistivity has been determined using current-voltage (I V) measurements using van der Pauw geometry. Electrical contact properties have been measured with various metals of different work functions, and the optimum Schottky barrier properties have been evaluated. Metal-semiconductor-metal (MSM) devices were fabricated and evaluated for radiation detector applications. Pulse height spectra (PHS) measurements were carried out using a ^{241}Am (59.6 keV) radiation source. Finally grown GaSe crystals were evaluated for THz sources and emission properties were determined. The results demonstrate that GaSe is a promising semiconductor for nuclear detection in Homeland security, nuclear non-proliferation, and nuclear power plants. The GaSe crystals also showed high potential as a TH$_Z$ source that could be used for imaging of concealed weapons, explosives, illicit drugs, chemical warfare, and biological agents.

TABLE OF CONTENTS

LIST OF TABLES

LIST OF FIGURES

LIST OF ABBREVIATIONS

CZT .... Cadmium Zinc Telluride

D.I. ....De-Ioninzed

eV ....Electron Volt

EDAX .... Energy Dispersive X-ray Spectroscopy

FWHM .... Full Width at Half Maxima

GaSe ....Gallium Selenide

GDMS .... Glow Discharge Mass Spectroscopy

I-V .... Current-Voltage

IED .... Improvised Explosive Devices

keV .... Kilo Electron Volt

MeV .... Mega Electron Volt

MCA .... Multi-Channel Analyzer

MSM ....Metal-Semiconductor-Metal

PHS ....Pulse Height Spectra

RT .... Room Temperature

RDD..Radiological Dispersal Devices

SEM .... Scanning Electron Microscopy

SIMPA .... Simultaneous Multiple Peak Analysis

SNM..Special Nuclear Material

THz .... Terahertz

VBM .... Vertical Bridgman Method

XRD ....X-Ray Diffraction

ZR .... Zone Refined

CHAPTER 1: GENERAL INTRODUCTION

1.1 INTRODUCTION

Nuclear terrorism risk is a major issue for the national security. There is a growing need for portable and high performance radiation detectors that can accurately identify the type, state, and location of illicit nuclear weapons, radiological dispersal devices (RDDs), and special nuclear materials (SNMs). Such detector would significantly reduce the time and cost required for screening at the ports-of-entry (shipping, airports, borders etc.), nuclear material accounting and safeguards, verification of non-proliferation treaty, and nuclear energy facility monitoring and accounting.

Nuclear decay of radioactive material produces various forms of radiations such as alpha particles, beta particles, gamma rays, x-rays, and neutrons. Nuclear detectors are semiconductor based devices that can identify, distinguish, and monitor sources of radiation produced by decay of radioactive isotopes. These nuclear radiations, depending on material properties, could ionize the semiconductor material in the detector device and produce charge carriers, which are then collected under an applied bias voltage and amplified to produce electrical signals. The semiconductor used for nuclear detector fabrication, its material properties, detector structure, and electronic instrumentation play important roles in fabricating high-resolution, high-efficiency nuclear detectors.

There are also considerable interests in employing Terahertz (THz) technology for detection and imaging of concealed weapons, explosives, chemical warfare agents, and

biological spores. THz radiation lies between the infrared and microwave portions of the electromagnetic spectrum. Terahertz radiation is also non-ionizing, and therefore not harmful to human tissue. The ability of THz radiation to penetrate many visually opaque materials and form high resolution images makes it ideally suited for detecting threats such as improvised explosive devices (IED), trafficking of illegal drugs, mails and packaging, corrugated cardboard, clothing, shoes, and other non-metallic objects. Furthermore, many explosives, chemical or biological agents, illicit drugs have characteristics spectral features in the THz range that can be used to identify these compounds.

Gallium selenide (GaSe), a nonlinear optical semiconductor with layered structure and wide bandgap, has many attributes of nuclear radiation detector and THz sensor. However, this wide bandgap semiconductor is little-studied and its potential has not been explored much. In this thesis, ultra-high purity GaSe single crystals were grown and different semiconductor material properties were investigated. Optoelectronic devices were then fabricated on grown GaSe crystals and tested for nuclear radiation detection and terahertz sensing applications.

1.2   THESIS OVERVIEW

Four major goals were achieved in this research work. The first goal was bulk growth of GaSe through a modified vertical Bridgman technique using high purity elemental precursors. The second goal was optical and electrical characterization of the grown crystals to understand crystal properties in terms of their effect on device performances. The third goal was to fabricate and study Ohmic and Schottky barrier

properties. Finally device performances were evaluated to asses' radiation detection and THz emission properties.

This thesis is divided into five chapters.

Chapter 1 provides significance of the work and motivation for GaSe semiconductor. A brief discussion of ideal and currently used semiconductor radiation detectors are provided. Then properties of GaSe and its potential as room-temperature direct read-out radiation detector is discussed. Also included is a brief discussion on THz emission properties and application of GaSe as TH_Z emitter.

Chapter 2 discusses crystal growth of GaSe crystals using a modified vertical Bridgman technique. First, purification of selenium (Se) precursor material by zone purification and subsequent impurity analysis by glow discharge mass spectroscopy is described. An overview of Bridgman growth technique along with the description and temperature profile of installed crystal growth furnace is provided. Growth of GaSe crystals from high purity elemental precursor materials with indium (In) and chromium (Cr) dopant and subsequent crystal processing is discussed.

Chapter 3 describes characterization of the grown crystals. The characterization comprises of structural characterization of GaSe crystals through powder x-ray diffraction (XRD) method, surface morphology evaluation through scanning electron microscopy (SEM), composition analysis in terms of stoichiometry through energy dispersive x-ray analysis (EDAX), optical absorption and transmission properties, and electrical resistivity measurements through current-voltage (I-V) measurements.

Chapter 4 is devoted to device fabrication and testing. This chapter described fabrication of monolithic metal-semiconductor-metal (MSM) detector structures of GaSe

using various metals of different work functions for Schottky contact analysis. A thermionic emission model has been used to study the Schottky contacts. The chapter also describes nuclear detector performance evaluations with [241]Am radiation source of 60 keV gamma energy and measurement of detection resolution from Pulse Height Spectra (PHS). Finally THz emission properties of GaSe are evaluated and discussed.

Chapter 5, the final chapter, concludes the findings of this work and gives suggestions for the future work.

1.3 BRIEF REVIEW OF EXISTING GAMMA-RADIATION DETECTORS

The most common radiation detector is the gas proportional counter or Geiger-Muller counter. Gas detectors require high pressure, high voltage to collect the ionization produced by incident nuclear radiation, and has long term stability problems. [1] Although it can detect alpha, beta, or gamma radiation, it cannot distinguish between them. Due to lack of specificity and good resolution, these detectors are mainly used for rough estimate of radioactivity

Currently high-purity germanium (HP Ge) detectors are the best performing and the most widely used gamma ray detectors with excellent energy resolution of ~ 0.2% for 662 keV benchmark gamma energy. [2] However due to low bandgap energy of Ge (0.67 eV at 300 K), Ge detectors require cryogenic cooling (<110K), which increases power consumption and makes the ConOps complicated. [3] Thereby, an ideal radiation detector would have high resolution as Ge detectors but would be able to operate at room temperature without any need of cooling system.

Cadmium zinc telluride, CZT, detectors have been developed as a room temperature alternative to Ge. [4-7] CZT is a good choice for nuclear detection due to its

wide bandgap energy to the range of 1.50 – 1.90 eV, high Z value of 52 (larger nucleus), and higher resistivity of 10^{10} Ω-cm. [8]   CZT detectors have shown ≤ 2% resolution at 662 keV at room temperature. [9]   However, a difficulty in growing large, high purity, and high quality crystals restricts its widespread use as a high energy gamma-ray detector.

Ge and CZT offer "direct read-out" operation, where electrical charge carriers generated by interaction of ionizing nuclear radiation is used to identify and measure the incident radiation.   There are other kind of materials known as scintillators, such as NaI(TI), where light is produced (not charge carrier) by interaction with nuclear radiation, and photomultiplier tube (PMT) or avalanche photodiodes (APD) are used to convert the light to electrical pulses.   Response speeds can be quite fast with some scintillators, but main drawbacks are low energy resolution. [10]   In general, solid-state "direct read-out" semiconductor detectors require only a few eV to create an electron-hole pair compared to 50 eV or more of energy in scintillators.   Thus in "direct read-out" detectors, a much greater detection signal is generated for a given amount of energy deposited resulting in better energy resolution.

Mercuric iodide (HgI_2) has high atomic numbers (Hg = 80 and I = 53) for high stopping power, and wide band-gap (2.13 eV at 300 K) for room temperature operation at low noise. [11]   Nonetheless, low charge collection efficiency in HgI_2 due to poor charge transport properties limits overall detection efficiency for this material. [12]   Furthermore HgI_2 is slightly hygroscopic and a very soft material requiring special encasement.

For Gamma ray detection, an ideal detector material would have high Z (larger nucleus) and higher density to stop high energy gamma rays, a wide bandgap for room

temperature applications and low thermal noise, high resistivity for low leakage current and thereby higher energy resolution, and high mobility lifetime product for higher sensitivity resulting in better charge collection efficiency.

1.4   MERIT OF GASE SEMICONDUCTOR AS GAMMA RAY DETECTOR

Gallium selenide (GaSe) is a III-VI semiconductor compound with layered hexagonal structure. Each monolayer is roughly 0.9-1.0 nm thick consisting of four-atom sequence of Se-Ga-Ga-Se. [13] The bonding within the layer planes is strong covalent, but the bonding between the interlayer is weak van der Waals, enabling cleaving of the semiconductor in layers. Due to this different crystallographic orientation along intra-layer and inter-layer directions, GaSe exhibits high anisotropy in its optical and electrical properties (unequal physical properties along different axes). [14] Figure 1.1 shows the anisotropic layered structure of GaSe crystals.
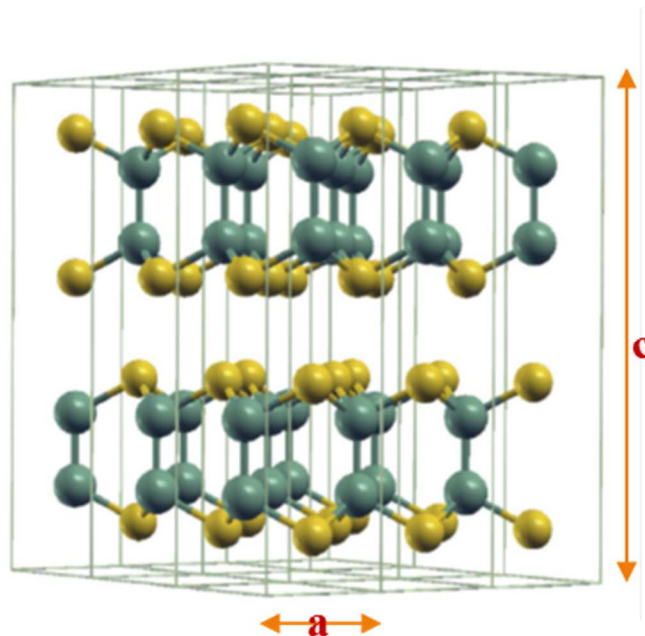

Figure 1.1. The crystal lattice of GaSe showing layered anisotropic structure (different structure along the axes); green spheres are Ga and yellow spheres are Se.

GaSe was first reported by Manfredotti et al. in 1974. [15]   Since then only limited number of papers have been published in this field. [16-20]. GaSe has high Z value of 34 (Z is the atomic number = the number of protons in the nucleus) for gamma stopping power. GaSe offers wide bandgap energy of ~ 2.0 eV at 300K that lies in the optical range of nuclear detector and facilitating room temperature operation, so there is no need for cooling arrangements making a compact system such as cryogenic cooling.

Detection efficiency, which measures the percentage of incident gamma radiation that was captured and amplified, is another important attribute of high performance gamma ray detector.   High purity and good quality GaSe crystals could increase collection efficiency of charge carriers produced by ionizing radiation by reducing carrier recombination or trapping, thereby improving the detection efficiency of gamma radiation. Thus, in order to develop high quality GaSe detectors, it is imperative to grow large, high purity and good quality crystals. Melting point of GaSe is 950°C and crystal cleaves easily, making the compound easier to grow at a moderate temperature and amenable to conventional material processing for device fabrication.

Table 1.1 lists selected physical and electrical properties of GaSe. In Table 1.2, desired qualities of GaSe semiconductor for room temperature gamma ray detection are listed and compared with various direct read-out detector materials.

Table 1.1 Physical and Structural Properties of GaSe at 300K

Crystal Structure:	Hexagonal
Lattice constant: a	3.743 Å
Lattice constant: c	15.916 Å
Molar Mass:	148.68 g/mol
Density:	5.3 g/cm^3; solid
Melting Point:	950°C
Band Gap:	2.02 eV @ 300K

Table 1.2 Properties of GaSe compared to other direct read-out radiation detectors

Semiconductor	Ideal	Ge	HgI$_2$	CdZnTe (CZT)	*GaSe*
Energy bandgap at 300K, E$_g$ (eV)	1.6 - 2.1	0.67	2.1	1.6 - 1.9	*2.0*
Atomic number, Z	>50	32	80, 53	52	*34*
Density (g/cm^3)	Solid	5.33	6.4	5.78	*5.03*
Resistivity (Ω-cm)	≥10^{10}	50	10^{12}	>10^{10}	*≥ 10^{10}*
Mobility, hole/electron μ (cm^2/V.s)	≥1000	1900/3900	4/100	50/1000	*uncertain*
Carrier lifetime, τ (μsec)	3	≥300	~2	~1	*minimal information*
Growth TEMP (°C)	700-1200	938	260	1175	*985*
Crystal growth and handling	Robust; Non-hygroscopic	Growable, excellent	Very soft; hygroscopic difficult to grow	Small crystal domains	*Growable; amenable to cleaving due to layered structure*

1.5   MERIT OF GaSe AS THz SENSOR

THz radiation lies in the intermediate frequency range between the infrared and microwave portions of the electromagnetic spectrum. This frequency range has not been widely utilized because of a lack of compact high power THz sources and high sensitivity detectors. In order to exploit THz radiation for threat detection applications, high power sources are required. Both peak power and average power could be significant, depending on the type of detector. In particular, the signal to noise ratio is proportional to the harmonic mean of the average and peak power of the source:

$$SNR \propto \sqrt{P_{average}P_{peak}} \equiv P_h \qquad\qquad 1.1$$

GaSe, a layered nonlinear optical semiconductor, has a number of exciting properties for nonlinear optical applications. Its broad transmission range (from 0.65 to 18 μm), with an absorption coefficient less than 1 cm^{-1} in the THz wavelength region, large nonlinear optical coefficient (d_{22} = 75 pm/V) and large figure of merit ($d_{eff}^2/n^3\alpha^2$ is a factor of ~9 x 10^4 larger than that of bulk LiNbO$_3$ at ~200 μm), and large birefringence make phase-matching accessible over a broad wavelength range. [21-23]

The ideal requirements for nonlinear optical materials are optical homogeneity, stability of the compound upon exposure to laser beam, and ease of fabrication. THz emission efficiency depends on the square of the length of the crystal. Thus to achieve high efficiency and high power output without sacrificing the optical quality, larger size crystals are needed. Another requirement is a higher quality crystal to reduce the amount of scattering and thereby improving the phase matching.

To develop high performance THz emitter, one need to: (i) identify and select optimum growth conditions to produce high quality crystals in a cost effective way; (ii)

9

develop pre-growth (purification) and post growth treatments to improve the optical quality of the grown crystal; and (iii) demonstrate that the grown crystals are capable of generating and detecting THz radiation with high efficiency at room temperature.

To address these needs, we have conducted experiments to grow large-area, high purity, and defect free gallium selenide (GaSe) single crystals for generating and detecting THz radiation in the 0.1 −10 THz range (10^{12} cycles/sec).

CHAPTER 2: GALLIUM SELENIDE CRYSTAL GROWTH

2.1 OVERVIEW

For both electrical devices (like nuclear detector) and optical devices (THz sensor) application, the semiconductor crystal, which the device is based on, must be of very high quality. Under high electrical field operation, impurities and native defects in semiconductor crystal may act as recombination or trapping centers and considerably deteriorate charge carrier transport properties and collection efficiency. These defects may lead to charge build up resulting a non-uniform electric response across the detector material. In case of THz, high quality GaSe crystals would reduce the amount of scattering, making the system more one dimensional and therefore narrow the transverse k spectrum of the THz radiation. This would improve the phase matching which in turn increase THz generation efficiency.

In this study, therefore, GaSe crystals were grown from highly pure (7N) Ga and Se precursors using a specially designed and computer operated crystal growth unit. Process modeling was carried out to determine the optimal growth conditions. One of the primary difficulties in GaSe crystal growth is its low thermal conductivity (0.37 W/mK) along the c-axis at close to the melting temperature. In addition, the thermal conductivity is anisotropic. An axial low temperature gradient was used to minimize the stresses (thereby structural defects) resulting from anisotropy of the thermal expansion.

2.2 Zone Purification of Selenium Precursor

Commercially available selenium material is of only 5N purity (99.999%). The presence of trace levels of residual impurities in commercially available Se precursor could intensely degrade the opto-electronic properties of grown GaSe crystals. Hence, zone refining (ZR) process was carried out on the commercially available Se to obtain Se material of ~ 7N purities (impurity at ppb level or lower). Since Ga precursor material of 7N purity was commercially available, no further zone purification was required for this element.

Zone refining technique relies on the idea that impurities are distributed differently in their solid and liquid phases at equilibrium.[24] The segregation coefficient *"k"* defines the relative concentration of impurities in the solid crystal compared to that of the melt:

$$k = \frac{C_s}{C_l} \qquad \qquad 2.1$$

where C_s is the impurity concentration in the solid phase and C_l is the impurity concentration in the liquid phase. A small segregation coefficient value (k < 1) implies that when a small zone of a material is melted and then re-solidifies very slowly, impurities in the material are segregated and majority of them remains in the melt.

Figure 2.1 shows a schematic of ZR setup with two ring heaters which travel one end to other end of the ampoule and illustrates the overall ZR process. A section (a zone) of the material at one end is melted with the ring heaters. As the heater travels very slowly from that end to the opposite end of the ampoule, the melted zone passes through the feed material. The segregated impurities, which are dissolved in the melt also get transported through the material from one end to other. Thus materials in one end

(starting side) become more pure and most of the impurities get accumulated in the finishing end. If this process is repeated multiple times, further purification of the material is achieved, and eventually a highly pure material is obtained. [25, 26]
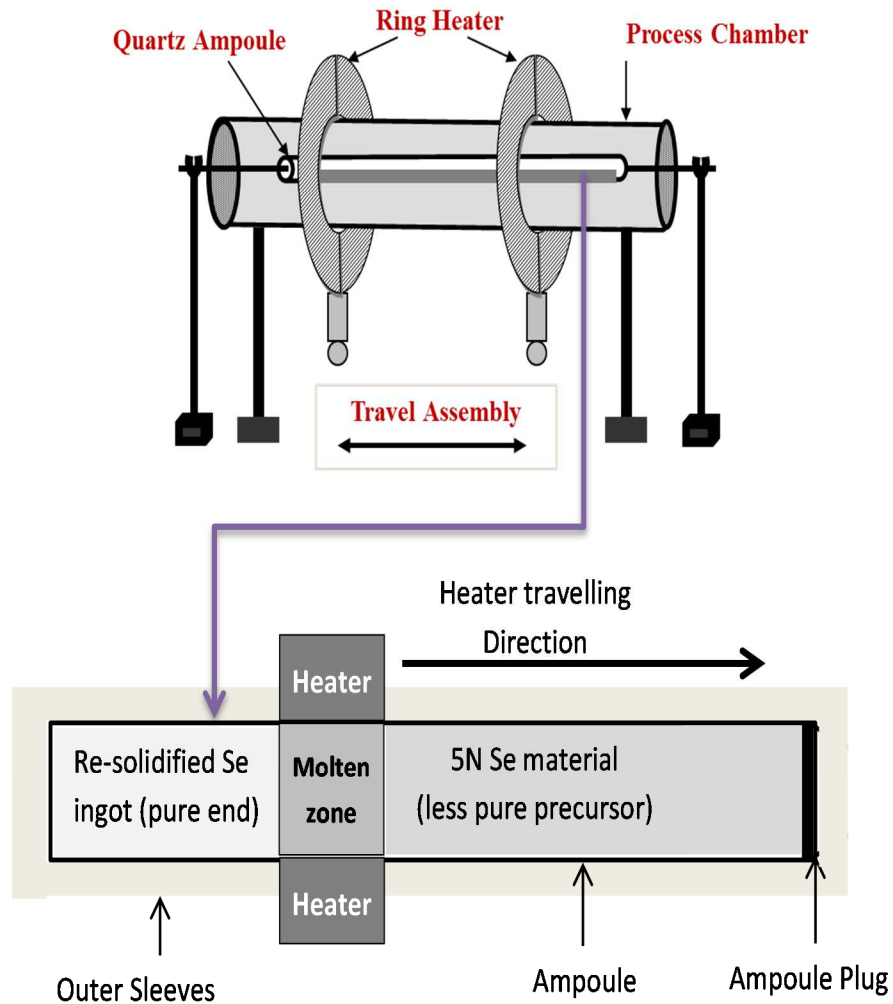

Figure 2.1. Schematic of horizontal zone refining process: (top) ZR setup with two ring heaters which travel along the ampoule length, and the bottom showing the solidified pure end, molten zone, and less pure end of precursor material.

Commercially available 5N selenium (Alpha Aesar) was purified using horizontal zone refining technique as shown above. Prior to ZR process, a quartz ampoule was thoroughly cleaned using successive washes with acetone, methanol, 10% HF aqueous solution, and de-ionized water (18 MΩ), and then baked overnight at 950°C under a constant nitrogen flow (~0.25 liter/min). The ampoule was loaded with 5N Se, sealed and then placed in the horizontal ZR system. Temperature controllers were used to maintain heater temperature at about 255°C little above the melting point of Se (221°C). The motion of the heater mounted on a track actuator was controlled at ~ 4 cm/hr using an Arduino electronics microcontroller.   Once the heater passed the entire length of ampoule (constitutes for one ZR pass), the heater was then quickly returned to its original position. About 40 ZR passes were carried out which took around 32 days.

In the post ZR, the ampoule was cut and the zone-refined material was removed inside an argon-controlled glove box. Depending on uniformity of shiny color, a length of ingot was considered 'pure' material, cropped from the impure end of the ingot, and stored in argon filled polyethylene bottles until they were ready to be used for crystal growth. The appearance of the zone refined Se ingots and synthesized Se beads are presented in Figure 2.2. Glow discharge mass spectroscopy (GDMS) has been used to identify and quantify the impurities in the Se precursor and ZR Se materials and the results are presented in Table 2.1. The data clearly demonstrated that most of the major impurity concentrations present in the commercially bought Se were reduced to ppb level or lower after zone purification.

| (a) | (b) |

Figure 2.2. (a) Appearance of the ZR Se ingots (~7N) after multi-pass zone purification; the shiny ingot at the extreme left is the purest end while ingot at the extreme right is the impure end. (b) Se dry pellets synthesized from the highly pure ZR ingots.

Table 2.1. Impurity analysis by GDMS showing reduction in elemental impurity concentration in Se material after zone-purification.

Element	Concentration before ZR	Concentration after ZR
Se	Major	Major
Hg	6-8 ppm	<4 ppb
Pb	16 ppm	<6 ppb
Sn	12 ppb	Not Detected
Ag	4-6 ppm	Not Detected
Cu	25 ppm	0.2 ppm
Fe	10 ppm	Not Detected
Mg	6 ppm	Not Detected
Si	4-6 ppm	0.4 ppm
Te	6-8 ppm	0.35 ppm

2.3 BRIDGMAN GROWTH OF GaSe CRYSTAL

GaSe crystals were grown by vertical Bridgman method (VBM) which involve melting the precursor material, and then crystallizing the material by changing pressure, temperature, or a combination of both in order to grow an ordered lattice structure.[8, 27] To form the covalent bonds that hold together the elements within the lattice structure, the growth temperature must be well above the melting point of the precursor elements as well as the compound being grown. The Bridgman technique uses a "hot" and "cold" zone to create a temperature difference within a furnace. The furnace has three temperature zones – (1) the upper zone with temperatures above the melting point of the crystal; (2) the lower zone with a temperature below melting point; and (3) an adiabatic zone between the two. A seed crystal is placed at the base of the growth ampoule. The precursor material melts at the hot zone. As the growth ampoule moves very slowly through the furnace, hot zone is translated into the cold zone and the molten precursor gets solidified along the crystalline direction of the seed crystal. Figure 2.3 shows pictures of ampoule sealing setup and in-house Bridgman growth furnace.

In Bridgman growth, melt flow and heat transfer is strongly coupled, thus ampoule pulling rate and rotation rate must be highly controlled to minimize the effect on temperature distribution. Process modeling studies on GaSe crystal growth was carried out using a crystal growth program as shown in

Figure 2.4. The modeling work was used to predict fluid flow pattern and temperature distributions and the relationship between the interface shape and growth conditions. The simulation shows when the melt convection is absent, the temperature

16

distribution is mainly determined by heat conduction.   Figure 2.5 shows schematic diagrams of Bridgman growth method along with the temperature profile.
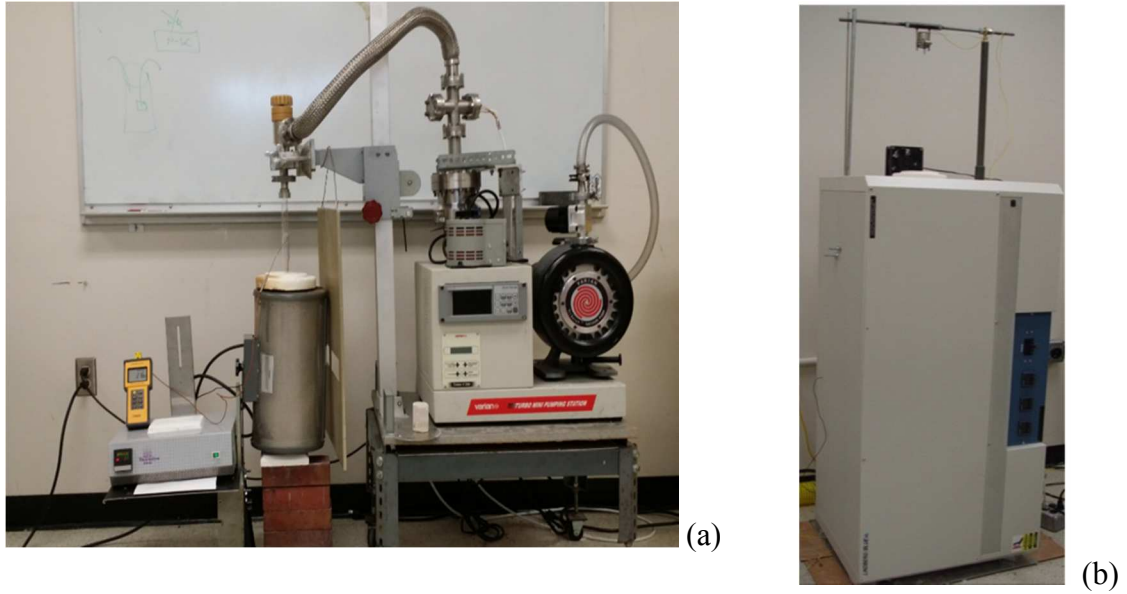

Figure 2.3. (a) Picture of a quartz ampoule sealing set up,   and   (b)   vertical   Bridgman growth furnace.
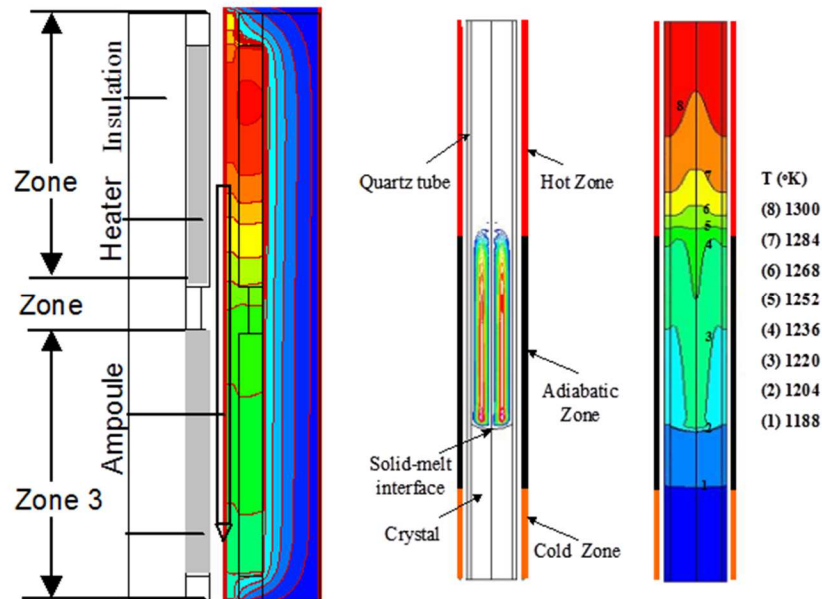

Figure 2.4. Temperature distribution of Bridgman furnace for growth of GaSe crystals.
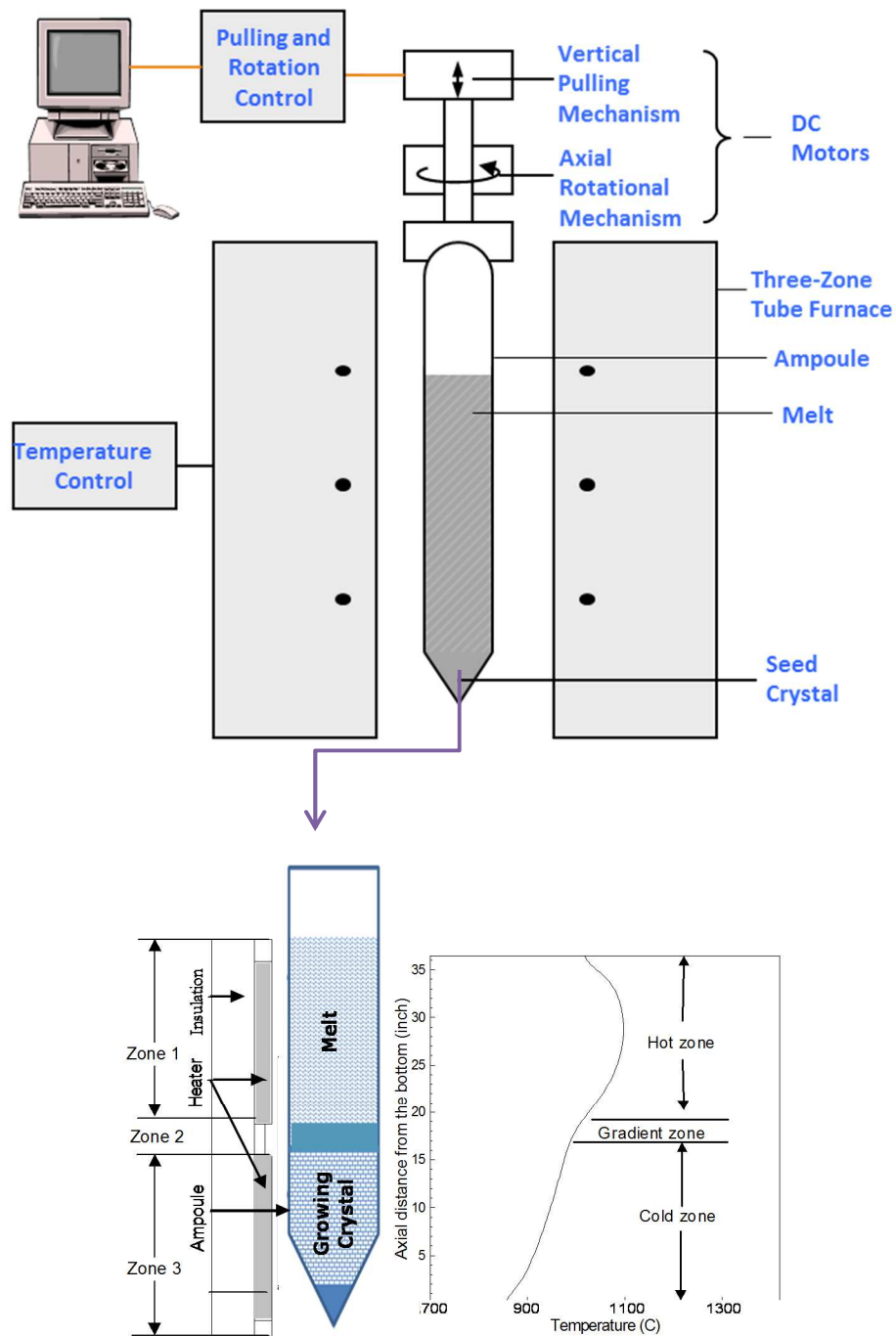
Figure 2.5. Schematic of an in-house crystal growth furnace with custom controlled pulling and rotation of the growth ampoule to ensure crystal quality and homogeneity (top). Schematic diagram and temperature profile of Bridgman method (bottom)

GaSe single crystals were grown from stoichiometric amounts of high purity (7N, Aldrich) Ga and zone-refined Se using a specially designed and computer operated crystal growth unit at USC. The precursor materials were weighed in stoichiometric amount for GaSe crystal growth, and were vacuum sealed at 10^{-6} torr in a cleaned carbon-coated quartz ampoule ($\geq$3 mm wall thickness). The quartz ampoule was sealed by dipping one end into liquid N_2 while sealing the other end. Dipping into the liquid N_2 was necessary because of the high vapor pressure of Se at the sealing temperature and also to avoid oxide formation. The sealed ampoule was then loaded in a horizontal-furnace for synthesis of GaSe polycrystalline compound at a temperature of about 1050°C.

The polycrystalline ingot was then placed in a conically tipped thick-walled ($\geq$3 mm) carbon coated quartz ampoule and sealed under a vacuum of 10^{-6} torr. The conical tip was designed to hold a GaSe seed crystal, which allowed growth along a preferred orientation. An axial low temperature gradient ($\sim$ 10 °C/cm at the growth zone) was imposed by tuning the input power distribution into the heater to stabilize the solid-liquid interface, to minimize stresses resulting from anisotropy of the thermal expansion coefficients, and also to suppress evaporation of Se. The sealed ampoule was suspended in the Bridgman crystal growth furnace and connected to a slow-speed (12 rpm) motor. Continuous rotation during the synthesis was used to ensure homogeneity. The polycrystalline material was heated slowly ($\sim$ 10 °C/hr) to 1050°C in a computer controlled vertical Bridgman growth furnace. The growth temperatures were maintained by temperature controllers. A computer-operated pre-programmed controller regulated the translational as well as rotational motion. The ampoule containing the melt moved

downward and the grown crystal was directionally solidified at a constant velocity of 0.5 cm/day.

After crystal growth, grown crystal ingot was retrieved from the quartz ampoule. The ingot was then cut carefully with a diamond wire-saw to obtain rectangular slices of GaSe. Figure 2.6 presents pictures of grown GaSe crystal ingot and a cleaved wafer. The cut crystal is then polished using a series of sandpapers of different grits and ultimately microfiber pads to achieve a mirror finish on all faces. Crystal wafers are then cleaned using an ultrasonicator, etched with 2% bromine-methanol solution (Br_2-MeOH) for 1 minute and 30 seconds, and rinsed off with de-ionized water. These wafers were then characterized prior to use as nuclear detectors and THz sources.
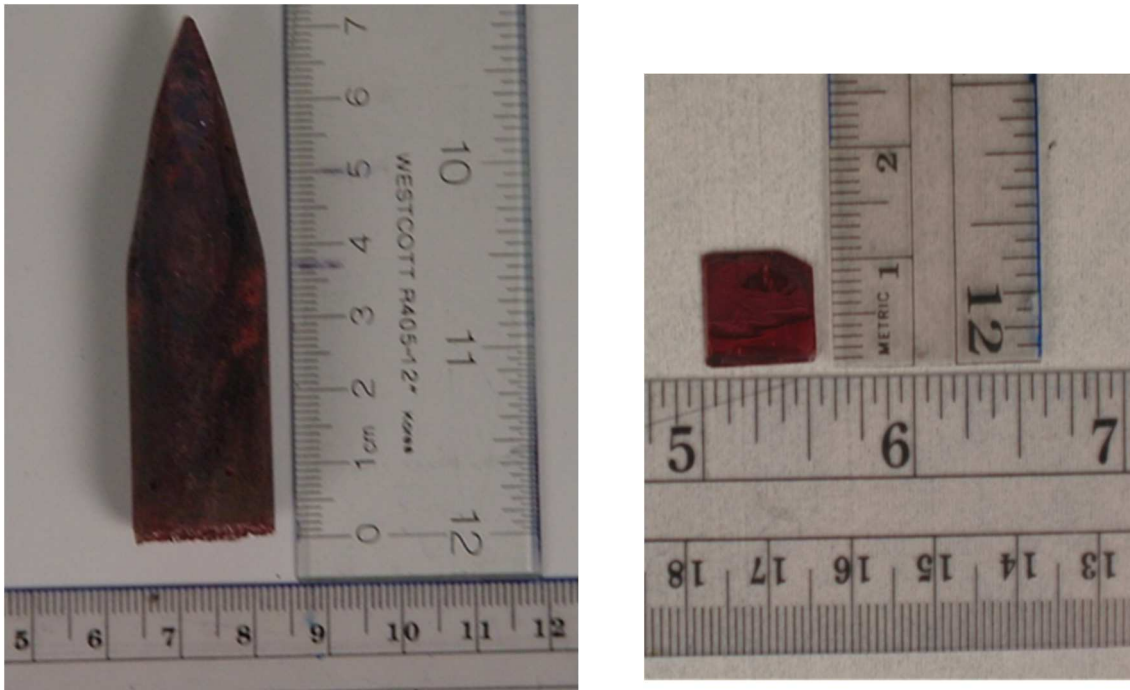

Figure 2.6. Typical picture of a grown GaSe crystal: (left) crystal ingot and (right) a cleaved wafer.

CHAPTER 3: GALLIUM SELENIDE CRYSTAL CHARACTERIZATION

3.1   OVERVIEW

A series of characterizations were carried out on grown GaSe crystals using scanning electron microscopy (SEM), x-ray diffraction (XRD), glow discharge mass spectroscopy (GDMS), optical absorption study, current-voltage (I-V) measurements to identify presence of any performance-limiting factors. The following subsections describe these characterization results.

3.2   SURFACE MORPHOLOGY STUDIES

Surface morphology studies were carried out to investigate the various crystallographic defects or irregularities such as grain boundaries, twins, and dislocations generated during the crystal growth and subsequent crystal processing. The surface morphology and microstructure of the grown crystals were examined by high-resolution scanning electron microscopy (SEM) studies with different magnifications. In SEM, the electron beam interacts with sample atoms, producing various signals that are collected to produce SEM image and electromagnets rather than lenses are used for focusing.   Figure 3.1 (a) shows SEM images of the surfaces of grown crystals.   The picture at left shows very smooth and shiny surfaces without any micro-cracks or defects (even with 550X magnification). The SEM picture at right shows layered structure of a cleaved GaSe sample.
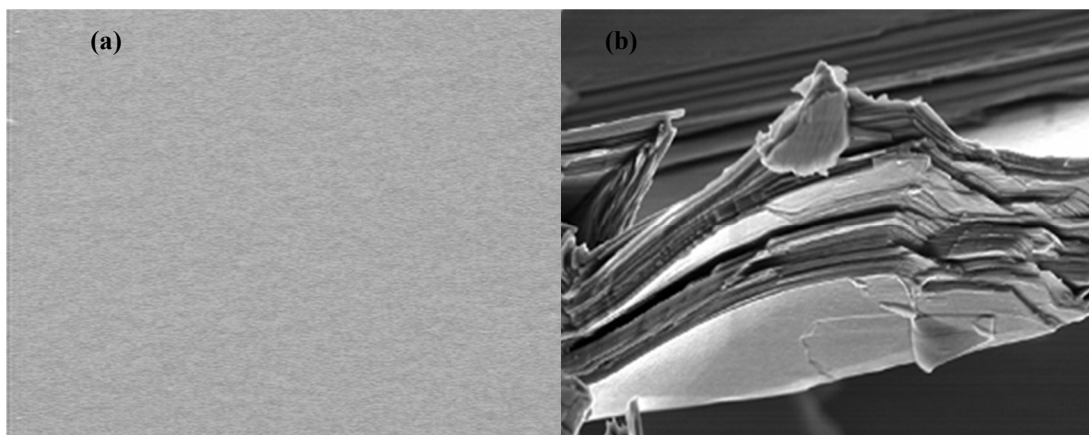
Figure 3.1. (a) SEM image (550× magnification) of a GaSe slice showing smooth, defect-free, and uniform crystal surface without any visible micro-cracks; (b) SEM image of a cleaved GaSe sample showing layered structure (400 × magnification).

3.3   COMPOSITIONAL CHARACTERIZATION

Elemental composition and the stoichiometry (Ga and Se atomic ratio) of the grown GaSe crystals were examined by scanning electron microscopy energy dispersive x-ray spectroscopy (SEM-EDAX).   In this method high energy electrons beam from SEM is used to excite the sample material in order to generate x-rays.   The incident electrons collide with inner shell electrons providing enough energy to emit x-ray photons.   The energies of these x-rays are distinctive of the elemental atom and contribute to the characteristic peaks on the EDAX spectra.   The element concentration is determined by integration of the peaks corresponding to the major elements present. [28]

Prior to SEM-EDAX analysis, the sample surface was prepared first by mechanical polishing with alumina suspension to obtain a mirror-finish.   The sample was then etched by applying the following cycle five times: 0.5% Br_2/MeOH dip for 20 seconds, ultrapure isopropanol rinse, and final drying by blowing pure nitrogen.   The

compositions of GaSe samples were determined using an FEI Quanta 200 Environmental Scanning Electron Microscope (ESEM) equipped with EDAX model NEW XL30 energy-dispersive X-ray spectrometer with Si (Li) detector.

EDAX analysis confirmed presence of Ga and Se elements in the GaSe crystals grown by the vertical Bridgman technique. The measurements were carried out on the different positions of wafers to demonstrate stoichiometric homogeneity across the crystal diameter. The average values of EDAX measurements for different GaSe crystal wafers are listed in Table 3.1. The results of these measurements showed a good stoichiometry and homogeneity across the wafer. A typical GaSe EDAX analysis spectrum is shown in Figure 3.2. The spectrum confirmed the presence of Ga and Se; Au peak is also observed because gold (Au) was deposited on the top surface to avoid surface charge effect.

Table 3.1. Compositions of GaSe crystals as determined by SEM-EDAX showing uniformity across the crystal wafers.

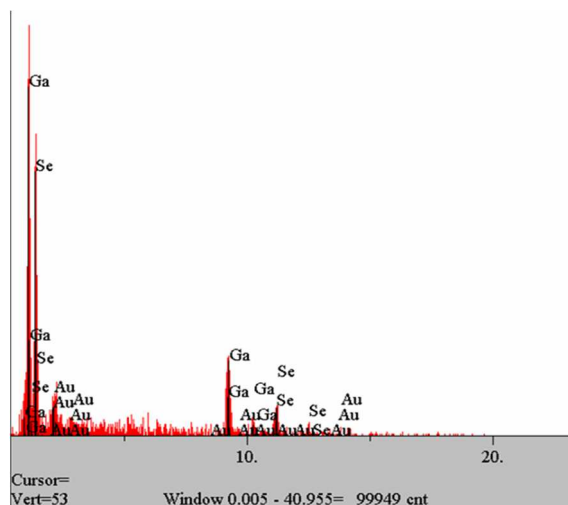|	Ga Cotent (at %)	Se Content (at %)
Spot #1	49.7	50.3
Spot #2	50.1	49.9
Spot #3	49.3	50.7

Figure 3.2. A typical EDAX spectrum of a grown GaSe crystal.

3.4 STRUCTURAL CHARACTERIZATION BY XRD

The structure and the formation of GaSe compound were confirmed by the X-ray diffraction (XRD) method. X-ray diffraction uses x-ray photons that interact with sample material and either get diffracted or transmitted depending on materials physical properties within a crystalline structure. This information is gathered by measuring the reflected or transmitted x-rays. Since materials have varying lattice spacing, arrangement, and composition, they diffract the incoming beam at different angles. These angles are then plotted with respect to their intensities.

The x-ray diffraction pattern was obtained using a Rigaku D/MAX 2100 powder x-ray diffractometer (CuK$_\alpha$ radiation, λ = 0.15406 nm). The sample was prepared for XRD measurement by grinding the crystal into a fine powder using a mortar and pestle. A typical XRD pattern of the powdered GaSe is shown in Figure 3.3. All the peaks were found to correspond to the GaSe compound. The x-ray powder diffraction results confirmed the hexagonal structure of GaSe with a = 3.743 Å and c = 15.916 Å. The unit cell lattice parameters derived from XRD pattern agree very well with literatures.

24

Assuming that the powdering of the crystal did not disturb the atomic arrangement within particles of the powder, the XRD result suggested that the grown crystals were monoclinic in structure.
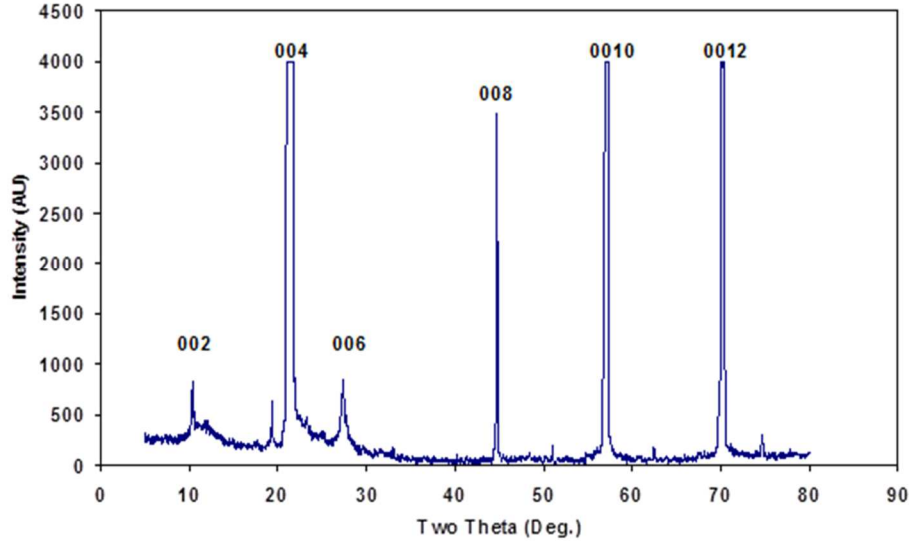

Figure 3.3. XRD patterns showing crystalline monoclinic structure of GaSe.

3.5   OPTICAL TRANSMISSION STUDY

Optical characterization was performed using UV-Vis spectroscopy to determine bandgap energy. For this study, transmission properties were measured from 500 nm to 1500 nm wavelengths using a thin (~ 30 μm thickness) GaSe wafer. The band gap energy, E_g, was calculated from the cut-off wavelength (λ) of the transmission spectrum, by using the following equation:

$$E_g(eV) = \frac{hc}{\lambda\ (microns)} = \frac{1.24}{\lambda\ (microns)} \qquad\qquad 3.1$$

where h is Planck's constant, c is the speed of light, E_g is the band gap of the GaSe crystal, and λ is the cut-off wavelength in microns. The optical transmission results for grown GaSe samples are shown in Figure 3.4. GaSe transmission spectrum

confirmed optical bandgap of ~2.02 eV at 300K.   The transmission spectrum above 600
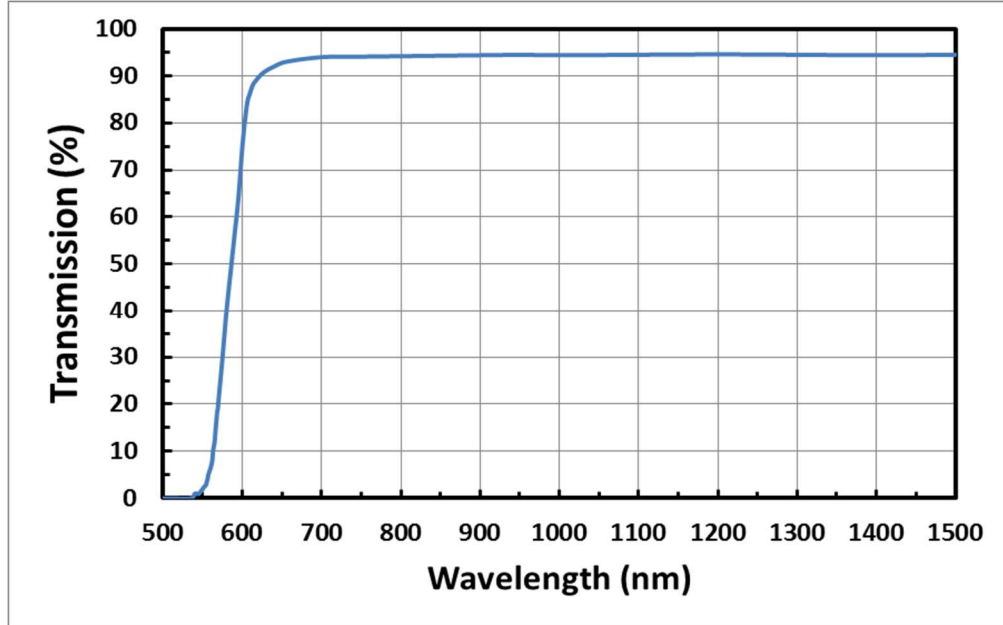
nm shows flat transmission of ≥ 90%.

Figure 3.4. Optical transmission spectrum of a grown GaSe crystal wafer.

3.6   CURRENT-VOLTAGE CHARACTERISTICS

The current-voltage (I-V) characterization is used to determine resistivity of the

grown GaSe crystal.   I-V measurement was carried out at room temperature using

Keithley 237 source and by measuring the current flowing through GaSe at various

applied voltages.   The electrical resistance was measured from inverse slope of the linear

regression of dark current-voltage curve.   The resistivity was calculated using the

equation below with known thickness and contact area:

$$\rho = R \cdot \frac{A}{L}$$

<div align="right">3.2</div>

where ρ is the resistivity of the crystal in Ohm-cm, R is the resistance in Ohms, A is the contact area (cm^2), and L is the thickness of the GaSe detector material.

A planar metal-semiconductor-metal (MSM) structure (In/GaSe/Au) was used to create a simple device for I-V measurements in order to determine resistivity. Figure 3.5 shows the current-voltage (I-V) characteristic of this device. The I-V characteristics show very low leakage current (a few nA at - 1000V) under dark condition. A high rectification ratio was observed with this particular device structure. The low leakage current at a very high bias is beneficial for detector performance because higher electric field can be applied to the detector without increasing noise and that will enhance the signal from a detector. The resistivity of the detector measured to be $\geq 10^{10}$ Ω-cm.
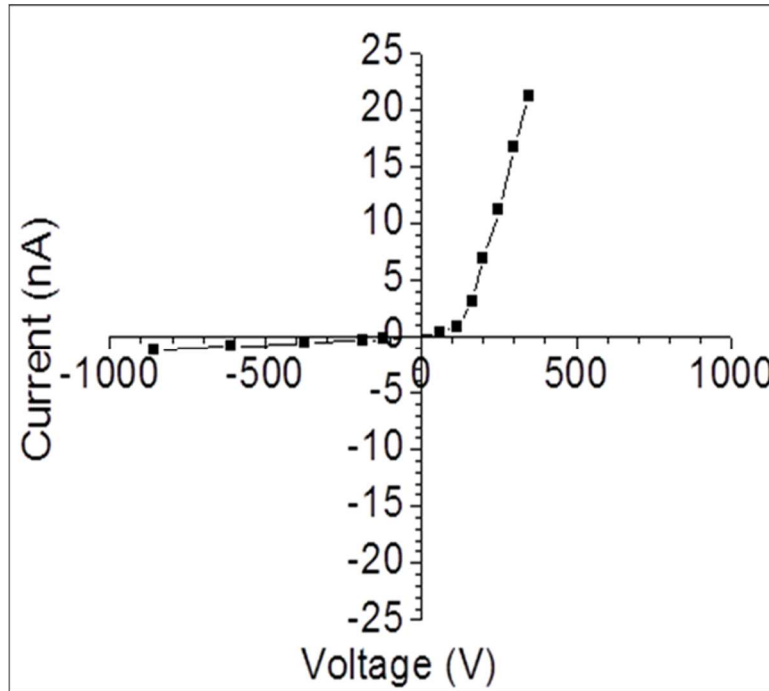

Figure 3.5. Current-voltage (I-V) characteristic of an In/GaSe/Au planar MSM detector.

CHAPTER 4: DEVICE FABRICATION AND CHARACTERIZATION

4.1   OVERVIEW

Using well characterized GaSe crystals, simple planner metal-semiconductor-metal devices were fabricated. Four different top metal contacts were investigated for rectifying Schottky contacts. Gold was used as the bottom contact for each cases. These detectors were further studied for their current-voltage properties in order to determine resistivity, barrier height, and dark leakage current. Nuclear detector performance was evaluated with ^{241}Am radiation source of 60 keV gamma-ray energy and detection resolution was measured from Pulse Height Spectra (PHS). Finally THz emission characteristics were determined for THz radiation in the 0.1 – 50 THz range.

4.2   GaSe DETECTOR FABRICATION

Rectangular slices of freshly cleaved from GaSe crystal ingot were used to fabricate planner metal-semiconductor-metal devices to evaluate electrical and spectroscopic properties of GaSe crystals. Metal contacts (electrodes) were deposited by sputtering (Figure 4.1) using a metal shadow mask. A semitransparent gold (Au) bottom electrode (150 – 180 Å thick) was deposited. For top electrode a variety of metals with different work functions were investigated. Thin (25 μm in diameter) palladium or copper wires were attached to the metal electrodes by applying small (1mm diameter) ag-paste or graphite suspension for connection to external electronics. A schematic of GaSe device is shown in Figure 4.2.

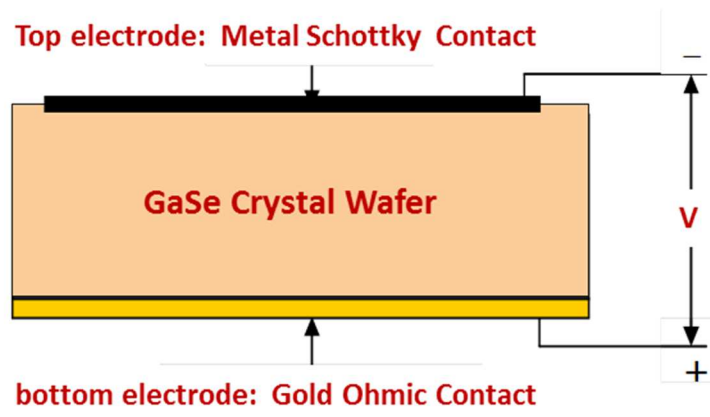Figure 4.1. RF/DC 13.56 MHz frequency sputtering unit used for metallization.

Figure 4.2. Schematic of simple plannar M-S-M device based on GaSe

4.3 METAL CONTACT STUDIES FOR SCHOTTKY DEVICES

For high resolution (low noise) devices, the choice of metal used for top contact electrode plays an important role in maintaining low leakage current under high bias conditions. The current-voltage characteristic (I-V characteristic) of a metal-semiconductor junction is determined by the barrier height at the interface. There are two

29

types of metal-semiconductor junctions: (i) Ohmic contact or non-rectifying contact, and (ii) Schottky contact or rectifying contact.

Ohmic contact contains very small contact resistance and current can flow in both biasing directions. In this type of contacts, ideally there is a linear relationship between Current and Voltage in reverse and forward bias. An Ohmic contact is formed when in (n-type) materials work function of metal $q\Phi_m$ is smaller than the work function of the semiconductor $q\Phi_s$. For p-type materials, it is formed when work function of the metal $q\Phi_m$ is larger than the work function of the semiconductor $q\Phi_s$. Figure 4.3 shows the energy band diagram of a non-rectifying (Ohmic) contact after thermal equilibrium for n-type and p-type semiconductor.
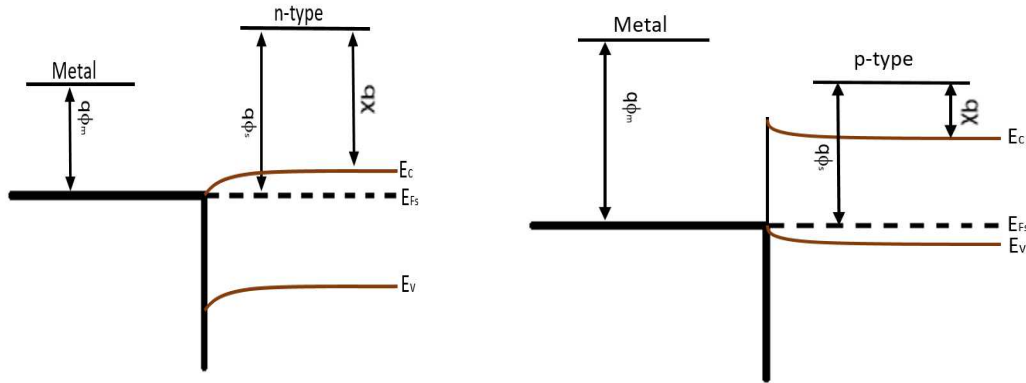

Figure 4.3. Band diagram of Ohmic contact with n-type (left) and p-type semiconductor (right) [29]

Schottky contact is formed when metal semiconductor has some rectifying effect. In this type of contact, current can only flow in one direction (forward bias) and there is low saturation current in the reverse bias. A Schottky barrier refers to a metal-semiconductor with a large barrier height ($\Phi_B > kT$). This type of contact forms when the work function of the metal $q\Phi_m$ is larger than the work function of the semiconductor $q\Phi_s$

for n-type semiconductors and in p-type semiconductors $q\Phi_m$ of the metal is smaller than

the $q\Phi_s$ of the semiconductor. [29] Figure 4.4 shows the energy band diagram for the

Schottky contact for n-type and p-type after the thermal equilibrium state.
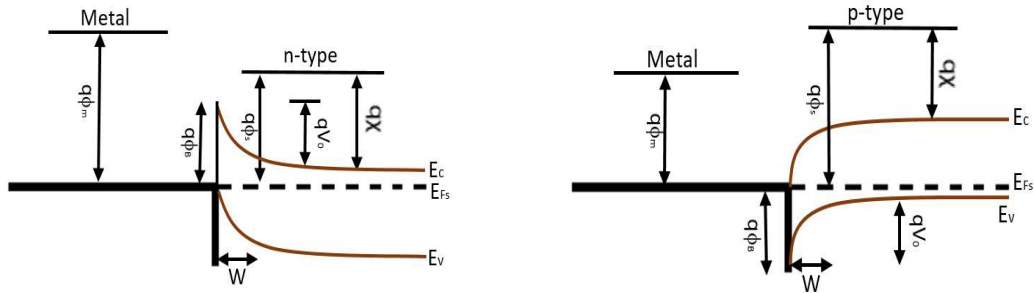

Figure 4.4 Band diagram of Schottky metal-semiconductor junction with n-type (left) and p-type semiconductor (right) [29]

The barrier height (ϕ_{bi}) at the metal-semiconductor interface is the difference

between metal work function (ϕ_m) and semiconductor work function (ϕ_s):

$$\phi_{bi} = \phi_m - \phi_s \qquad\qquad 4.1$$

$$q\phi_{bi} = q\phi_m - q\chi \qquad\qquad 4.2$$

where χ is the electron affinity which is required to remove an electron from the

conduction band to vacuum level.

The voltage dependent junction current in a Schottky contact can be expressed as:

$$I = I_s(e^{\frac{\beta V}{n}} - 1) \qquad\qquad 4.3$$

Using logarithm, the Equation 4.3 could be written as:

$$log(I) = \frac{\beta V}{n} + log(I_s) \qquad\qquad 4.4$$

31

where I_S is the saturation current, V is the applied voltage, n is the diode ideality factor, $\beta = q/k_BT$, q being the electronic charge (1.6×10^{-19} C), k_B the Boltzmann constant (8.62×10^{-5} eV/K), and T is the absolute temperature (°K). The saturation current is:

$$I_S = A^*AT^2\left(e^{-\beta\varphi_B}\right) \qquad 4.5$$

where A is the area of the diode, φ_B is the Schottky barrier height, and A^* is the effective Richardson constant which can be expressed as:

$$A^* = 4\pi^2\ m^*/h^3 = 120\ (m^*/m)\ Acm^{-2}\ K^{-2} \qquad 4.6$$

where h is Planck constant, and m* is the electron effective mass. [30, 31] Using current measurements at varying applied voltage and then plotting log(I) versus applied voltage bias, one could measure the ideality factor 'n' from the slope and saturation current I_s from the intercept.[32, 33]

The junction properties between GaSe and four different metals with varying work functions (Au, Ni, Ag, In) were investigated using current-voltage measurements. The aim was to investigate whether the choice of metal can improve the performance of the detector by minimizing the dark leakage current. Current-voltage (I-V) characteristics of various metals contacts were carried out and are shown in

Figure 4.5. I-V characteristics were carried out at room temperature using a Keithly 237 electrometer setup. Among the four metal contacts tested, only indium (In) contact showed diode characteristics with high rectification. I-V characteristics in general showed very low leakage currents in the reverse biases as well as forward biases.

The type of contact (Ohmic or Schottky) formed with these metal top contacts are tabulated in Table 4.1.

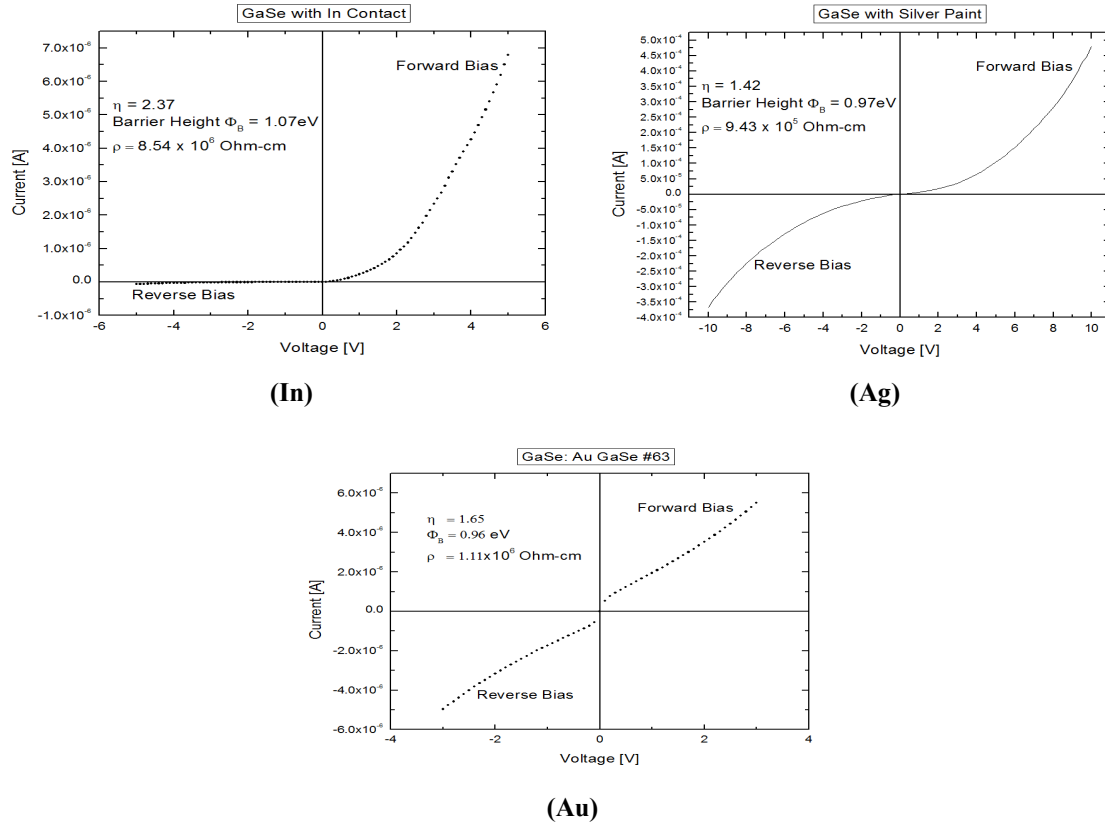**(In)**

(Ag)

(Au)

Figure 4.5. Current-voltage characteristics of various metals contact junction with GaSe. Only the junction with indium showing high rectification.

Table 4.1. Contact formation of GaSe with different metal contacts for top electrode

Metal	Metal Work Function	Contact Formation
Indium (In)	4.09	Rectifying or Schottky
Nickel (Ni)	5.15 eV	Non-Rectifying or Ohmic
Gold (Au)	5.1 eV	Non-Rectifying or Ohmic
Silver Paint (Ag)	4.26-4.74 eV	Ohmic contact observed

33

4.4 RADIATION TESTING

In this study, GaSe detectors were developed for detection of gamma radiation (frequencies of above 10^{19} Hz) produced by decay of nuclear materials. The incident gamma radiations produce fast moving electrons within the GaSe detector material. These fast moving electrons are collected at the anode electrode by applying an external voltage bias, inducing an electrical charge signal. Preamplifiers then converts charge signal to a voltage signal, next shaping amplifier filters noises, and finally multi-channel analyzers (MCA) converts analog signals into digital signal and provide pulse height spectra (PHS) corresponding to the incident gamma radiation.

The radiation detection setup used for this thesis work is shown in Figure 4.6. An ^{241}Am radioisotopes were used as nuclear source to irradiate the detector. ^{241}Am provides low-energy gamma-rays at 59.6 keV or alpha particles at 5.486 MeV. The GaSe detector and the radiation source were housed in an aluminum RFI/EMI shielded test box. Canberra 3106D high voltage supply was used to bias the GaSe radiation detector. The test box was connected in sequence to an Amptek A250CF preamplifier, an Ortec 671 spectroscopic shaping amplifier, an oscilloscope and finally to a Canberra Multiport IIe multi-channel analyzer. Data from the multi-channel analyzer is sent to the Genie 2000 PC software, which generates the pulse height spectrum. The energy resolution of the detector is calculated from the pulse height spectrum at full-width- half-maxima (FWHM) of Gaussian peak fitting using the following equation;

$$\% \, Energy \, Resolution = \frac{FWHM \, (keV)}{Incident \, Energy \, (keV)} * 100\% \qquad 4.7$$

34

Lower values of energy resolution and FWHM indicate better detector performance. Figure 4.7 shows a pulse height spectrum of planar M-S-M GaSe radiation detector under [241]Am radiation source.   After performing Gaussian peak fitting, the FWHM of the gamma photopeak at ~59.6 keV was calculated to be ~4.8%
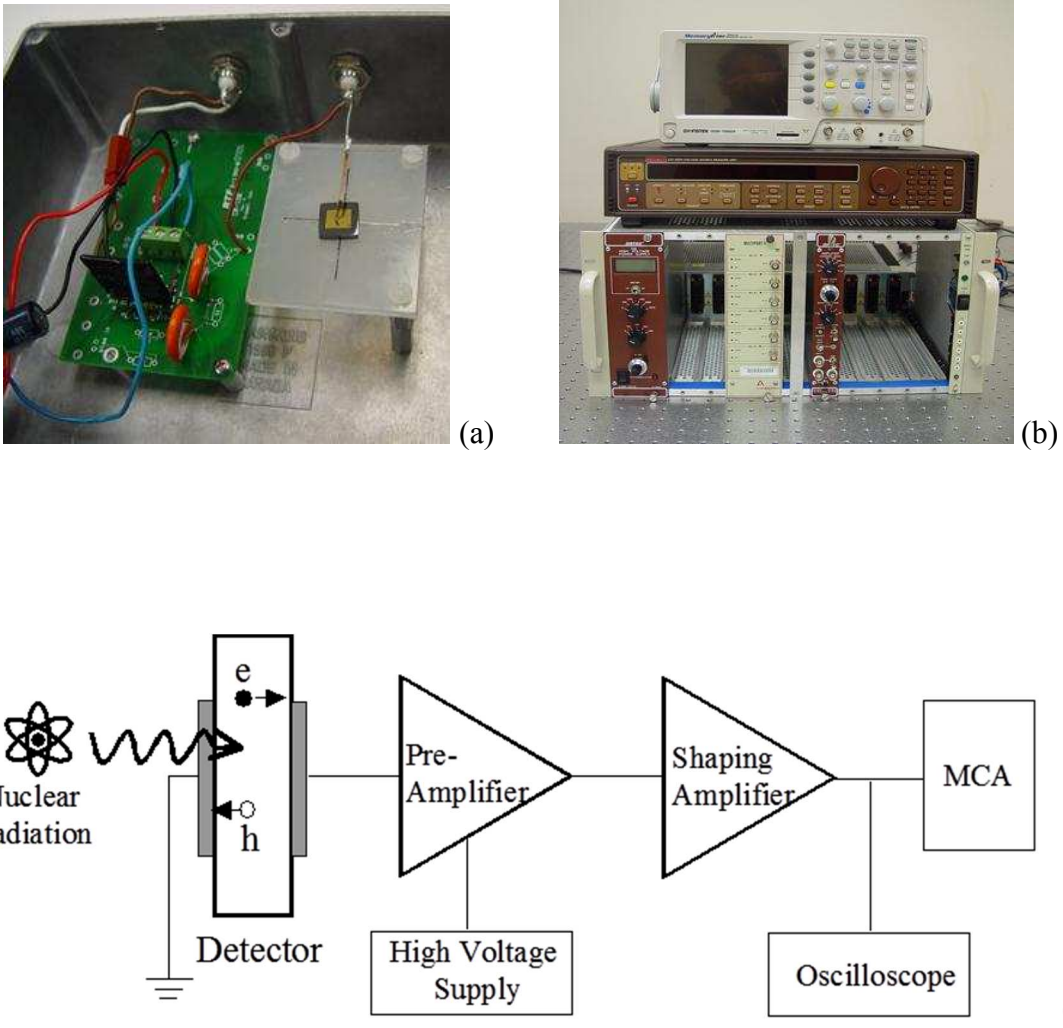

Figure 4.6. Pictures of the shielded aluminum testing box with a detector (a) and radiation detection system (b); a schematic of the detection measurement system (c).
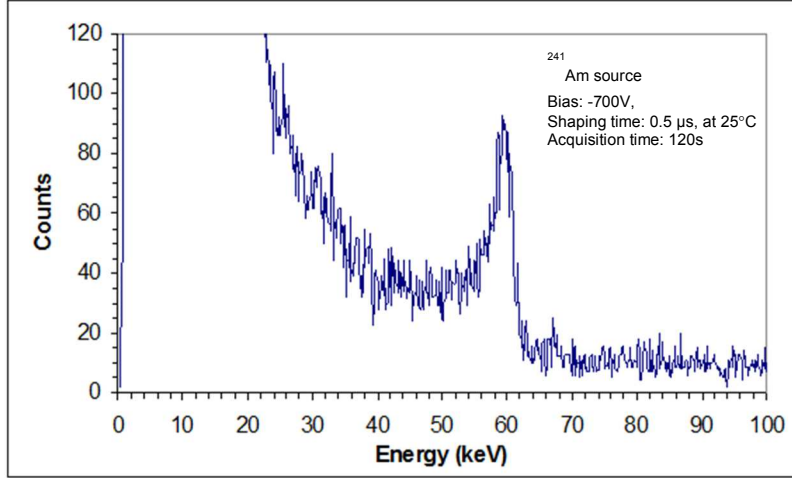
Figure 4.7. Pulse height spectrum (PHS) of the GaSe detector with a resolution of 4.8% at 59.6 keV using a [241]Am radiation source.

4.5 THz TESTING

The time-domain THz emission measurement setup that was used for this work is an optical pump-probe arrangement. Experimental arrangements for terahertz time domain spectroscopy (THz-TDS) system used to explore the THz radiation characteristics of GaSe as shown in Figure 4.8. A commercial diode-pumped titanium-sapphire (Ti:S) laser which delivers pulses with a duration from of 10-fs at a wavelength of 800 nm with 350 mW average power was used as an optical source. The laser beam is split into a pump beam and a probe beam using an uncoated glass as beam splitter. The power ratio is typically 95% on the pump beam and 5% on the probe beam. THz emission from unbiased semiconductor surfaces is achieved by exposing the surface to the pump light beam. Two off-axis parabolic mirrors were used to collect and refocus the THz wave. For comparison, a <110> ZnTe crystal was used as a reference sensor.
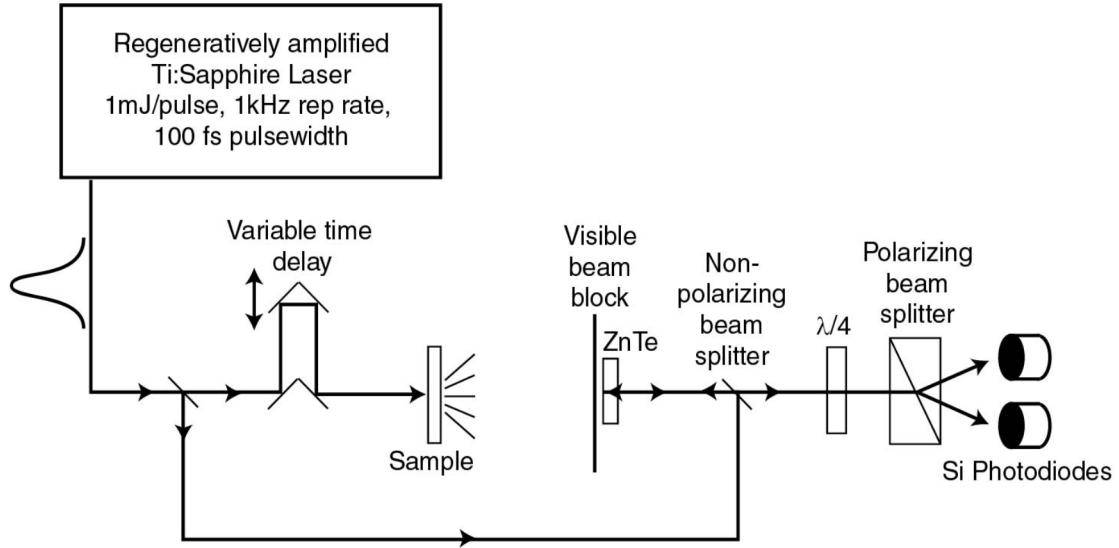
36

Figure 4.8. Schematic experimental setup for terahertz time domain spectroscopy (THz-TDS) system used to explore the THz radiation characteristics of GaSe.[34]

Typical frequency domain THz waveform spectrum generated from a GaSe crystal during the THz-TDS measurement is shown in Figure 4.9. along with a **s**pectrum generated by ZnTe standard crystal. The GaSe crystals showed high potential as THz sources and THz emission properties of 0.3 to 32 THz has been found. The THz wave peak signal detected with the GaSe was about four times larger compared to the THz peak measured with the reference ZnTe.
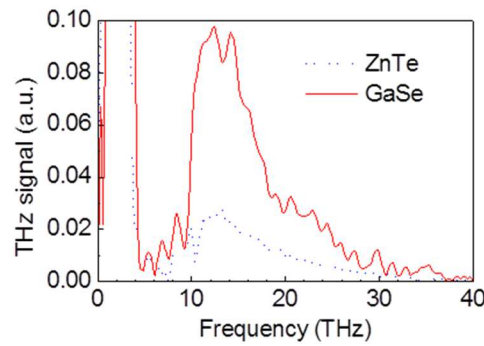

Figure 4.9. The Normalized Frequency domain THz Spectra of GaSe [34]

CHAPTER 5: CONCLUSION AND FUTURE WORK

5.1 CONCLUSION

GaSe crystal was grown from zone refined ultra-pure precursor materials using modified multi-pass vertical Bridgman growth furnace. A series of characterization were carried out on grown crystals including scanning electron microscopy (SEM), x-ray diffraction (XRD), energy dispersive x-ray spectroscopy (EDAX), optical absorption study, and current-voltage (I-V) measurements.   These extensive characterizations provided information on stoichiometry, morphology, purity, bandgap energy, resistivity, and presence of any performance-limiting electrical defect.

Grown GaSe crystals had smooth, defect-free layered structure as determined by SEM and XRD. The XRD results also confirmed the hexagonal structure of GaSe with a = 3.743 Å and c = 15.916 Å.   Elemental composition and the stoichiometry (Ga and Se atomic ratio) of the grown GaSe crystals were to be $Ga_{0.5}Se_{0.5}$ as determined by SEM-EDAX.   The bandgap of the crystals was found to be 2.02 eV at 300K by optical transmission, which is in the correct range for detector-grade GaSe. The   transmission spectrum   above   600   nm   shows   flat   transmission   of $\geq$ 90%;   this   large optical window will be beneficial for THz emission.   The electrical resistivity was estimated to be 10^{10} Ω-cm, which is high enough to fabricate a functional radiation detector.

Different metal-semiconductor contacts with metals of various work functions and metal-semiconductor-metal (MSM) devices with planar structures have been studied to ensure good charge transport properties and opto-electronic device performances. The GaSe detectors showed very low leakage current at a high bias (below 5 nA at – 1000V) due to their high resistivity, which are beneficial for high resolution detectors. The barrier height for In/GaSe/Au Schottky contact was found to be ~1.1 eV and the diode ideality factor was measured to be 2.37, which is higher than unity showing the presence of deep levels as traps and recombination centers.

Finally, GaSe detectors were tested for gamma ray nuclear detector and THz emission applications. The fabricated GaSe detector devices were evaluated with ^{241}Am (5.5 MeV) radiation source. An energy resolution of 4.8% was obtained for GaSe planar detector. Typical frequency domain THz waveform spectrum generated from a GaSe crystal showed high potential as THz sources and THz emission property of 0.3 to 32 THz has been found. The THz wave peak signal detected with the GaSe was about four times larger compared to the THz peak measured with the reference ZnTe.

5.2 FUTURE WORK

To fabricate high resolution and high sensitivity GaSe devices, future efforts should be concentrated on growing large area single crystals. To improve the opto-electronic and charge transport properties, in-detailed investigations should be carried out using deep-level transient spectroscopy (DLTS) and thermally stimulated current spectroscopy (TSC) to identify principal impurities, various point defects, and deep-level defects. For radiation detector performance, study should be carried out with high energy radiation sources such as ^{137}Cs (662 keV). For high energy resolution, detector structures

such as guard-ring, coplanar grids, or Frisch collar should be explored. A detailed surface chemical analysis such as x-ray photoelectron spectroscopy (XPS) and transmission electron microscopy (TEM) will be essential to optimize the optical and electrical performance of the devices. The long-term optical emission characteristics through THz measurements need to be investigated.

REFERENCES

[1]   B. Milbrath, A. Peurrung, M. Bliss, and W. Weber, "Radiation detector materials: An overview," *Journal of Materials Research*, vol. 23, pp. 2561-2581, 2008.

[2]   G. Knoll, "*Radiation Detection and Measurement*," 3rd ed., New York: John Wiley and Sons, 2000.

[3]   P. N. Luke, R. H. Pehl, and F. A. Dilmanian, "A 140-element Ge detector fabricated with amorphous Ge blocking contacts," *IEEE Trans. Nucl. Sci.,* vol. 41, pp. 976-978, 1994.

[4]   S. D. Sordo, L. Abbene, E. Caroli, A. M. Mancini, A. Zappetteni, and P. Ubertini, "Progress in the Development of CdTe and CdZnTe Semiconductor Radiation Detectors for Astrophysical and Medical Applications," *Sensors,* vol. 9, pp. 3491-3526, 2009.

[5]   Sandeep K. Chaudhuri, Khai Nguyen, Rahmi O. Pak, Liviu Matei, Vladimir Buliga, Michael Groza, Arnold Burger, and Krishna C. Mandal, "Large Area $Cd_{0.9}Zn_{0.1}Te$ Pixelated Detector: Fabrication and Characterization," *IEEE Trans. Nucl. Sci.*, vol. 61, pp. 793-798, 2014.

[6]   R. M. Krishna, S. K. Chaudhuri, K. J. Zavalla, and K. C. Mandal, "Characterization of $Cd_{0.9}Zn_{0.1}Te$ based virtual Frisch grid detectors for high energy gamma ray detection," *Nucl. Instrum. Methods Phys. Res. A,* vol. 701, pp. 208-213, 2013.

[7]   R. O. Pak and K. C. Mandal, "Defect Levels in Nuclear Detector Grade $Cd_{0.9}Zn_{0.1}Te$ Crystals," *ECS J. Solid State Sci. Technol.*, vol. 5, pp. P3037-P3040, 2016.

[8]   K. C. Mandal, S. H. Kang, M. Choi, A. Kargar, M. J. Harrison, D. S. McGregor, A. E. Bolotnikov, G. A. Carini, G. C. Camarda, and R. B. James, *IEEE Trans. Nucl. Sci.*, vol. 54, pp. 802-806, 2007.

[9]   A. E. Bolotnikov, K. Ackley, G. S. Camarda, C. Chercher, Y. Cui, G. De Geronimo, J. Fried, D. Hodges, A. Hossain, W. Lee, G. Mahler, M. Maritato, M. Petryk, U. Roy, C. Salwen, E. Vernon, G. Yang, and R. B. James, "An array of virtual Frisch-grid CdZnTe detectors and a front-end application-specific integrated circuit for large-area position-sensitive gamma-ray cameras," *Rev. Sci. Instrum,* vol. 86, pp. 073114-1-5, 2015.

[10] S. E. Pfanstiel, K. J. Hofstetter, and T. A. DeVol, "Comparison of four types of gamma- and X-ray detectors for environmental applications in the 10-450 keV energy range," *J. Radioanal. Nucl. Chem.*, vol. 223, pp. 89-98, 1997.

[11] W. R. Willig, "Mercury iodide as a gamma spectrometer," *Nuclear Instruments and Methods*, vol. 96, pp. 615-616, 1971.

[12] K. Hull, A. Beyerle, B. Lopez, J. Markakis, C. Ortale, W. Schnepple, L. van den Berg, "Recent Developments in Thick Mercuric Iodide Spectrometers," *IEEE Trans. Nucl. Sci.*, vol. 30, pp. 402-404, 1983.

[13] V. G. Dmitriev, G. G. Gurzadyhan, and D. N. Nikogosyan, *Handbook of Nonlinear Optical Crystals*, Springer, New York, 1999.

[14] C. Manfredotti, R. Murri, A. Quirini, and L. Vasanelli, "A Particular application of GaSe semiconductor detectors in the neutrino experiment at CERN," *Nucl. Instr. and Meth.*, vol. 131, pp. 457-462, 1975.

[15] C. Manfredotti, R. Murri, and L. Vasanelli, "GaSe as nuclear particle detector," *Nucl. Instr. and Meth.*, vol. 115, pp. 349-353, 1974.

[16] E. Sakai, H. Nakatani, C. Tatsuyama, and F. Takeda, "Average energy needed to produce an electron-hole pair in GaSe nuclear particle detectors," *IEEE Trans. Nucl. Sci.*, vol. 35, pp. 85-88, 1988.

[17] H. Nakatani, E. Sakai, C. Tatsuyama, and F. Takeda, "GaSe nuclear particle detectors," *Nucl. Instr. and Meth. A*, vol. 283, pp. 303-309, 1989.

[18] T. Yamazaki, K. Terayama, T. Shimazaki, and H. Naktani, "Impurity-doped GaSe radiation detector evaluated at 100 °C," *Jpn. J. Appl. Phys.*, vol. 36, pp. 378-379, 1997.

[19] B. L. Yu, F. Zeng, V. Kartazayev, R. R. Alfano, and Krishna C. Mandal, "Terahertz studies of the dielectric response and second-order phonons in a GaSe crystal," *Appl. Phys. Lett.*, vol. 87, pp. 182104-1-3, 2005.

[20] Krishna C. Mandal, C. Noblitt, M. Choi, A. Smirnov, and R. David Rauh, "Crystal growth, characterization and anisotropic electrical properties of GaSe single crystals for THz source and radiation detector applications," *AIP Proc.*, Vol. CP772, pp. 159-160, 2005.

[21] N. C. Fernelius, "Properties of gallium selenide single crystal," *Prog. Crystal Growth and Charact.*, vol. 28, pp. 275-353, 1994.

[22] W. Shi, Y. J. Ding, N. Fernelius, and K. Vodopyanov, "Efficient, tunable, and coherent 0.18-5.27 THz source based on GaSe crystal," *Opt. Lett.*, vol. 27, 1454-1456, 2002.

[23] R. Huber, A. Brodschelm, F. Tauser, and A. Leitenstorfer, "Generation and field-resolved detection of femtosecond electromagnetic pulses tunable up to 41 THz," *Appl. Phys. Lett.*, vol. 76, 3191-3193, 2000.

[24] K. C. Mandal, A. Mehta, S. K. Chaudhuri, Y. Cui, M. Groza, and A. Burger, "Characterization of amorphous selenium alloy detectors for x-rays and high-energy nuclear radiation detection," *SPIE Proc.*, vol. 8852, pp. 88521O-1-7, 2013.

[25] W. R. Wilcox, Zone Refining, Kirk-Othmer Encyclopedia of Chemical Technology, John Wiley & Sons, 2001.

[26] *Zone Refining, McGraw-Hill Science & Technology Encyclopedia, The McGraw-Hill Companies, Inc., 2005.*

[27] S. D. Sordo, L. Abbene, E. Caroli, A. M. Mancini, A. Zappetteni, and P. Ubertini, "Progress in the Development of CdTe and CdZnTe Semiconductor Radiation Detectors for Astrophysical and Medical Applications," *Sensors,* vol. 9, pp. 3491-3526, 2009.

[28] Amit C. Das, Sayantan Bhattacharya, Mukesh Jewariya, Shriganesh Prabhu, Krishna C. Mandal, Tsuneyuki Ozaki, and Prasanta Kumar Datta, *IEEE J. Selected Topics in Quantum Electronics*, vol. 23, pp. 1-7, 2017.

[29] B. G. Streetman and S. K. Banerjee, Solid state electronic devices, Upper Saddle River: Prentice Hall, 2006

[30] N. Mott, Electronic Processes in Non-crystalline Materials, Oxford: Clarendon Press, 1979.

[31] Donald A. Neamen, Semiconductor Physics and Devices Basic Principles, 4th ed., McGraw Hill, 2007.

[32] Krishna C. Mandal, Peter G. Muzykov, Sandeep K. Chaudhuri, and J. Russell Terry, "Low energy x-ray and γ-ray detectors fabricated on n-type 4H-SiC epitaxial layer," *IEEE Trans. Nucl. Sci.,* vol. 60, pp. 2888-2893, 2013.

[33] Sandeep K. Chaudhuri, Kelvin J. Zavalla, and Krishna C. Mandal, "High Resolution Alpha Particle Detection Using 4H-SiC Epitaxial Layers: Fabrication, Characterization, and Noise Analysis," Nuclear Instrum. Methods in Physics Research A, vol. 728, pp. 97-101, 2013.

[34] Krishna C. Mandal, Sung H. Kang, Michael Choi, Jian Chen, X. –C. Zhang, James M. Schleicher, Charles A. Schmuttenmaer, and Nils C. Fernelius*," IEEE Journal of Selected Topics in Quantum Electronics,"* vol. 14, pp. 284-288, 2008.

43